Determination of the Momentum Distribution from the Dynamic Structure Factor in Quantum Liquids

J. J. Weinstein and J. W. Negele

Center for Theoretical Physics, Laboratory for Nuclear Science, Department of Physics, Massachusetts Institute of Technology, Cambridge, Massachusetts 02139

(Received 22 July 1982)

Scaling of the dynamic structure factor at high momentum transfer is established by using time-ordered perturbation theory. Whereas the scaling function is the longitudinal momentum distribution for systems interacting with smooth two-body potentials, additional terms contribute in the case of strong short-range repulsion. Illustrative results are presented for a hard-sphere Bose gas and the relevance to electron scattering from nuclei and neutron scattering from liquid helium is discussed.

PACS numbers: 67.40.Db, 61.12.Fy

The dynamic structure factor, $S(\vec{q},\omega)$, has been measured by electron scattering from nuclei[1] and neutron scattering from liquid helium.[2] In the impulse approximation,[3] it is directly related to the momentum distribution, $n(\vec{p})$, by

$$qS(\vec{q},\omega) \approx m \int \frac{d^3p}{(2\pi)^2}\, \delta(\vec{p}\cdot\hat{q} - y) n(\vec{p}), \qquad (1)$$

where

$$y \equiv m\omega/q - q/2. \qquad (2)$$

Because of the importance of an unambiguous experimental determination of the momentum distribution in dense quantum liquids like liquid helium and nuclear matter, this work addresses the general relation between $S(\vec{q},\omega)$ and $n(\vec{p})$ and the particular features which arise for two-body potentials having strongly repulsive cores at short range.

The structure factor may be expressed as

$$S(\vec{q},\omega) = \pi^{-1}\,\mathrm{Im}\int_0^T dt\, e^{i\omega t}\, i\langle \hat{\rho}(\vec{q},t)\hat{\rho}(-\vec{q},0)\rangle, \qquad (3)$$

where $\hat{\rho}(\vec{q},t)$ is the Fourier transform of the Heisenberg density operator at time t. One means of enumerating systematic corrections to Eq. (1) is the expansion of $\hat{\rho}(\vec{q},t)\hat{\rho}(-\vec{q},0)$ as a sum of many-body operators to be evaluated at equal time, giving rise to sums of integrals of many-body correlation functions.[4] For repulsive cores, however, serious inconsistencies arise since interactions in the time interval $(0,t)$ are treated perturbatively whereas those outside this interval are summed to all orders in the ground-state wave function. Further assumptions to enable evaluation of the correlation functions then yield uncontrolled approximations.

To treat interactions inside and outside the interval $(0,t)$ equivalently, it is useful to express the perturbation expansion of Eq. (3) in terms of time-ordered diagrams.[5,6] A selected set of low-order diagrams is given in Fig. 1, where the lower dot with an incoming arrow denotes excitation with momentum $\vec{q}$ at time 0, the upper dot with an outgoing arrow indicates removal of momentum $\vec{q}$ at time t, upgoing and downgoing lines indicate particle and hole propagators, respectively, all

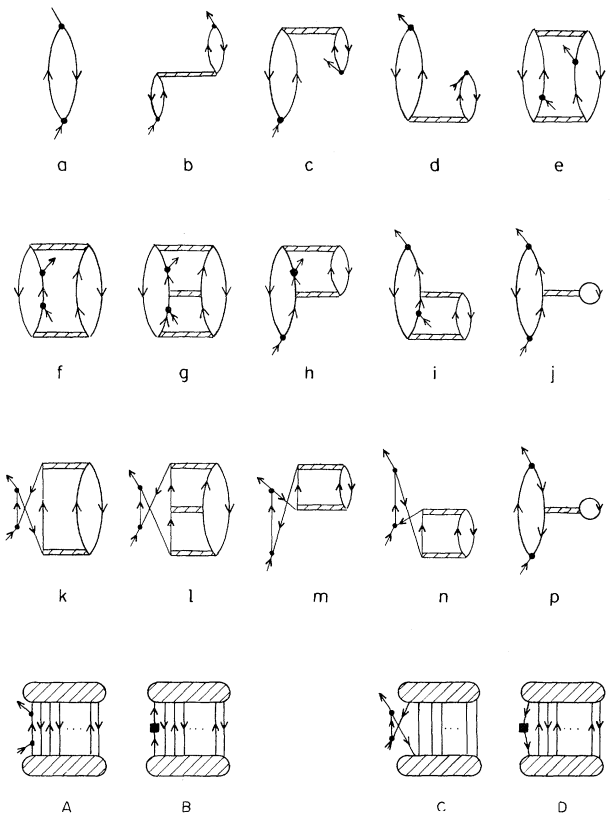

FIG. 1. Time-ordered diagrams contributing to the dynamic structure factor and momentum distribution as defined in the text.

distinct exchange graphs for each diagram are to be included, and the shaded rectangles should be temporarily regarded as two-body interactions.

For smooth potentials, having Fourier transforms which decrease exponentially in q, it is straightforward to demonstrate scaling in the variable y,[7] that is that the limit as $q \to \infty$ of $qS(\vec{q}, \omega = qy/m + q^2/2m)$ approaches a function of y. The $\vec{q}$ dependence of each diagram is analyzed as follows. Unless the $\vec{q}$ injected at time 0 can flow solely through particle propagators to be removed at time t, the diagram vanishes at least exponentially in q. The q dependence of the remaining diagrams arises from propagators in the interval $(0,t)$ which have energy denominators of the form

$$E = \omega - \sum_{\text{particles}} \epsilon + \sum_{\text{holes}} \epsilon + i\eta = \omega - \epsilon_{\vec{p}+\vec{q}} + C + i\eta$$
$$= (q/m)[y - \vec{p}\cdot\hat{q} + O(1/q)] + i\eta, \quad (4)$$

where $\vec{p}$ denotes the momentum of the particle or hole receiving excitation q at time 0 and C denotes all other q-independent particle and hole energies. Diagrams having no interactions during $(0,t)$, such as a, f, and k in Fig. 1, thus have a single denominator of form (4) yielding an imaginary part

$$(m/q)\delta(y - \vec{p}\cdot\hat{q} + O(1/q));$$

diagrams like b, g–j, and l–p with one interaction are of order $1/q^2$; and those with m interactions are of order q^{-m-1}. The most general contributions of order $1/q$ to $S(q, \omega = qy/m + q^2/2m)$ are of the generic form shown in diagrams A and C at the bottom of Fig. 1, where the shaded regions denote arbitrary multiparticle-multihole amplitudes. Comparison with the corresponding generic form for general contributions to the momentum distribution B and D indicates that individual diagrams differ only by the one-body momentum operator, denoted by the square box, and the factor $(m/q)\delta(y - \vec{p}\cdot\hat{q} + O(1/q))$, where $\vec{p}$ is the particle momentum in A and B and the hole momentum in C and D. Thus, in all orders of perturbation theory, it is observed that in the large-q limit, $qS(\vec{q}, \omega = qy/m + q^2/2m)$ approaches the impulse-approximation result, Eq. (1), and thus scales in y.

The q dependence described above is crucially altered for two-body potentials with strongly repulsive cores. We consider first the idealized case of an infinitely repulsive hard core of radius a. The total cross section approaches a constant and hence, by the optical theorem, the imaginary part of the forward scattering amplitude grows linearly with q. In addition, off the energy shell the real part of the forward scattering amplitude may also be shown to have linear q dependence.[6,8] The perturbation series for S must be resummed and the diagrams in Fig. 1 actually represent all contributions of first and second order in the hole-line expansion which are nonvanishing for $q > 2k_F$ with the shaded rectangles denoting G matrices. Note, as remarked at the outset, that contributions inside and outside the time interval $(0,t)$ are treated consistently in each order of the expansion, as for example in diagrams f–j. The q counting of the original analysis is modified by an additional power of q for each forward scattering of a particle line carrying q. Diagrams g and j each require such an additional factor q and thus contribute in leading order. Diagrams k–p are most conveniently evaluated by using generalized time ordering[8] by which it may be shown that the sum $k+l+m$ is of order $1/q$ whereas $n+p$ is of order $1/q^2$. The final result is that $qS(q, \omega = qy/m + q^2/2m)$ scales to a function of y, but because of nonvanishing contributions from diagrams g–j the scaling function no longer is related to the momentum distribution via Eq. (1). The analogous result for bosons is obtained from the fermion result utilizing the high-spin technique[9] of defining a fictitious spin with degeneracy equal to the particle number and projecting onto a spin singlet which forces the spatial wave function to be totally symmetric.

To assess the quantitative significance of the additional terms g–j all two-hole–line contributions to the structure factor were calculated numerically for bosons interacting through a pure hard-core potential of radius a. The results, reduced to dimensionless form, are shown for several values of momentum transfer in Fig. 2 and compared with the impulse approximation, Eq. (1), using $n(\vec{p})$ calculated to the same order in the hole-line expansion. Because random-phase-approximation diagrams, which are crucial for the low-momentum behavior of Bose systems, are omitted from the present calculation, the results should only be considered for $y > (8\pi \times a\rho)^{1/2}$. The essential result is that in the range of momenta considered in Fig. 2 the impulse approximation, denoted IA, overestimates the full result in the high-q limit, denoted $\tilde{q} \approx \infty$, by from 40% to 60%. Thus, although qS scales and displays symmetry about $y = 0$, properties often presented as evidence for the validity of the impulse

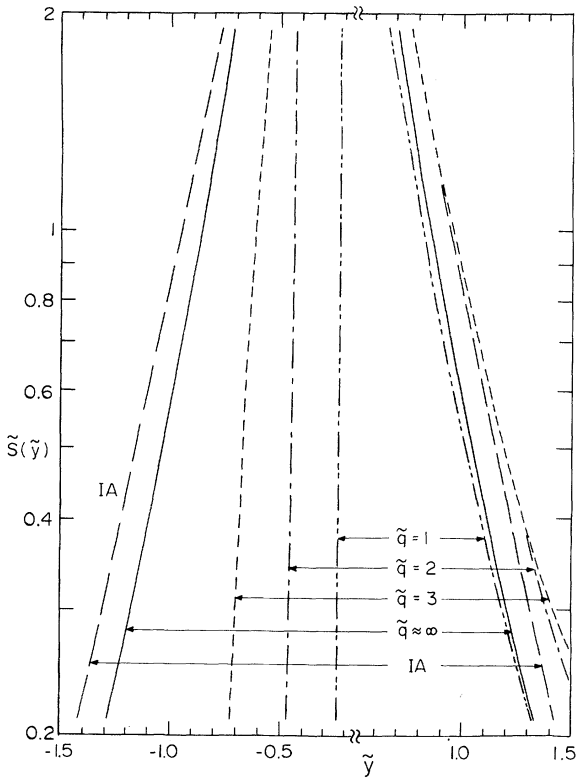

FIG. 2. The structure factor $\hat{S}=qS(\boldsymbol{q},\omega=qy/m+q^2/2m)/\rho ma^4$ as a function of $\tilde{y}=ya$. The momentum transfer is specified by $\tilde{q}=qa$ and IA denotes the impulse approximation using Eq. (1).

approximation, extraction of a momentum distribution from it via Eq. (1) would lead to error of the order of 50%.

Finally, it is desirable to comment on the relevance of the hard-core results to liquid helium and nuclei. At scattering energies corresponding to the range of momentum transfer for which scaling analyses are performed, helium-helium and nucleus-nucleus total cross sections are roughly constant, implying that the imaginary part of the forward scattering amplitude must grow roughly linearly with q. Phenomenological potentials, such as the Lennard-Jones[10] and Reid[11] potentials, reflect this same behavior in their strongly repulsive cores. Thus, in the relevant momentum transfer region, diagrams g–j should be qualitatively as important as for the hard-core case and produce quantitatively significant deviations from the impulse approximation. These deviations are particularly pertinent to the recent effort to determine the momentum distribution of liquid ^{4}He by assuming the validity of the impulse approximation for neutron scattering.[12] Because of the limitation to $y>(8\pi a\rho)^{1/2}$, the present calculation unfortunately is not directly applicable to the interesting problem of determining the zero-momentum condensate fraction.

In the case of liquid helium, neutron scattering experiments extend up to $\tilde{q}=qa\sim 45$. In the calculations in Fig. 2 the scaling limit has essentially been reached at $\tilde{q}=45$, with results at $\tilde{q}=30$ differing negligibly on the scale of the figure. Even the lower-momentum-transfer data of Ref. 12 correspond to $\tilde{q}\sim 15$, which is reasonably close to the scaling domain. In contrast, electron scattering experiments from nuclei extend only to $\tilde{q}\sim 3$ which is far from converging to the scaling limit. Note, however, that because of oscillating exchange terms, there is misleading apparent convergence for positive y near $q=3$, at which point qS stops increasing and begins decreasing toward the $\tilde{q}\sim\infty$ limit.

For liquid ^{4}He Monte Carlo techniques for bosons have been used to evaluate the momentum distribution[13] and can be used to calculate Euclidean correlation functions for density operators $\rho(\vec{q})$ acting at two different imaginary times. If practical methods can be developed to continue stochastically evaluated Euclidean correlation functions to real time, an exact calculation of the dynamic structure function can be compared with the impulse approximation for a realistic potential, eliminating the restrictions of the present calculation to two-hole–line contributions and hard cores. In the case of electron scattering, the complications of the full two-body interaction, Fermi statistics, relativistic corrections, and spin and current contributions to scattering render quantitative calculations impractical, but the present analysis suggests that extraction of the momentum distribution from qS will be complicated by short-range repulsive interactions to at least the same extent as in liquid helium.

This work was supported in part by the U. S. Department of Energy under Contract No. DE-AC02-76ER03069.

[1]I. Sick, D. Day, and J. S. McCarthy, Phys. Rev. Lett. 45, 871 (1980).
[2]H. W. Jackson, Phys. Rev. A 10, 278 (1974).
[3]P. C. Hohenberg and P. M. Platzman, Phys. Rev. 152, 198 (1966).
[4]H. A. Gersch, L. J. Rodriguez, and P. N. Smith, Phys. Rev. A 5, 1547 (1972), and 8, 905 (1973).
[5]J. Goldstone, Proc. Roy. Soc. London, Ser. A 239, 267 (1952).
[6]J. Weinstein, Ph.D. dissertation, Massachusetts

Institute of Technology (unpublished).
[7]G. West, Phys. Rep. 18C, 263 (1975).
[8]H. A. Bethe, B. H. Brandow, and A. G. Petschek, Phys. Rev. 129, 225 (1963).
[9]B. H. Brandow, Ann. Phys. (N.Y.) 64, 21 (1971).
[10]R. D. Murphy and R. O. Watts, J. Low Temp. Phys. 2, 510 (1970).
[11]R. V. Reid, Ann. Phys. (N.Y.) 50, 411 (1968).
[12]V. F. Sears, E. C. Svensson, P. Martel, and A. D. B. Woods, Phys. Rev. Lett. 49, 279 (1982).
[13]M. H. Kalos, M. A. Lee, P. A. Whitlock, and G. V. Chester, Phys. Rev. B 24, 115 (1981).

Incommensurate-Reentrant High-Symmetry Phase Transition in a Layer-Structure Perovskite

P. Muralt, R. Kind, and R. Blinc [a]

Laboratory of Solid State Physics, Swiss Federal Institute of Technology, Hönggerberg, CH-8093 Zürich, Switzerland

and

B. Zeks

J. Stefan Institute, E. Kardelj University of Ljubljana, Ljubljana, Yugoslavia

(Received 5 April 1982)

In contrast to the usual structural "lock-in" incommensurate-commensurate transitions—where the amplitude of the modulation wave continues to increase at T_c but the incommensurate part of the average wave vector of the modulation wave vanishes—in $(C_3H_7NH_3)_2MnCl_4$ the amplitude of the incommensurate modulation wave vanishes outside T_{c1} and T_{c2} whereas the wave vector is not critical. This reentrant behavior results from a coupling of the incommensurate order parameter to the temperature-dependent interlayer distance.

PACS numbers: 64.60.-i

The phase-transition sequence commonly observed[1] in structurally incommensurate systems is as follows: high-temperature disordered phase (P)—incommensurately modulated ordered phase (I)—commensurate ordered phase (C). The P-I transition is the result of a condensation of a soft mode with a wave vector which is incommensurate to the periodicity of the underlying lattice, whereas at the I-C transition the frozen-out modulation wave becomes commensurate, i.e., the average wave vector "locks in" to the basic lattice. Here we report on a thermal dilatation-induced incommensurate-reentrant high-symmetry phase transition in normal and partially deuterated $(C_3H_7NH_3)_2MnCl_4$ (abbreviated as C3Mn) where the *amplitude* of the modulation wave and *not* the incommensurate part of the average wave vector vanishes (Fig. 1) with lowering temperature. This phenomenon has so far not been observed in other incommensurate systems.

C3Mn is a pseudo-two-dimensional perovskite where layers of corner-sharing $MnCl_6^-$ octahedra are sandwiched between rigid—but dynamically disordered—propylammonium chains.[2,3] In the high-temperature α phase (space group $I4/mmm$) the propylammonium groups are reorienting around their long axes between four equivalent orientations. In the partially ordered β phase the

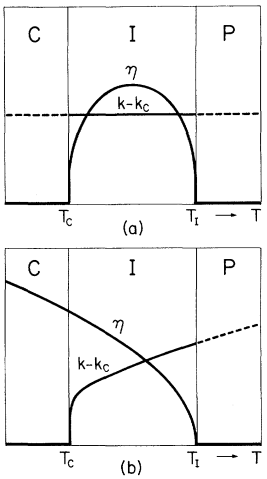

FIG. 1. Schematic temperature dependence of the amplitude (η) and the average incommensurate wave vector (k-k_c) in (a) C3Mn and (b) a "normal" incommensurate system in the P, I, and C phases.